J. Fluid Mech. (2011), *vol.* 672, *pp.* 358–383.
doi:10.1017/S0022112010005975

Contact lines over random topographical substrates. Part 1. Statics

NIKOS SAVVA[1], GRIGORIOS A. PAVLIOTIS[2] AND SERAFIM KALLIADASIS[1]†

[1]Department of Chemical Engineering, Imperial College London, London SW7 2AZ, UK

[2]Department of Mathematics, Imperial College London, London SW7 2AZ, UK

(Received 23 March 2010; revised 22 October 2010; accepted 16 November 2010; first published online 11 February 2011)

We investigate theoretically the statistics of the equilibria of two-dimensional droplets over random topographical substrates. The substrates are appropriately represented as families of certain stationary random functions parametrized by a characteristic amplitude and wavenumber. In the limit of shallow topographies and small contact angles, a linearization about the flat-substrate equilibrium reveals that the droplet footprint is adequately approximated by a zero-mean, normally distributed random variable. The theoretical analysis of the statistics of droplet shift along the substrate is highly non-trivial. However, for weakly asymmetric substrates it can be shown analytically that the droplet shift approaches a Cauchy random variable; for fully asymmetric substrates its probability density is obtained via Padé approximants. Generalization to arbitrary stationary random functions does not change qualitatively the behaviour of the statistics with respect to the characteristic amplitude and wavenumber of the substrate. Our theoretical results are verified by numerical experiments, which also suggest that on average a random substrate neither enhances nor reduces droplet wetting. To address the question of the influence of substrate roughness on wetting, a stability analysis of the equilibria must be performed so that we can distinguish between stable and unstable equilibria, which in turn requires modelling the dynamics. This is the subject of Part 2 of this study.

Key words: contact lines, drops, thin films

1. Introduction

The problem of wetting of a solid substrate by a liquid has been an active topic of both applied and fundamental research for several decades (see Dussan V. 1979; de Gennes 1985; Blake 1993; Bonn *et al.* 2009, for detailed reviews). Wetting phenomena are characterized by the presence of a three-phase contact line where the substrate, liquid and surrounding gas meet. Often substrates are not smooth but are characterized by topographical features with a wide range of length scales, from the micro- to the macro-scale. Small-scale irregular features, often referred to as 'roughness', are naturally present in all surfaces, unless they are specially treated. The presence of topography can have a profound effect on contact lines and wetting. This problem has attracted considerable attention in the last few years primarily due to newly emerging technologies such as self-cleaning substrates (Blossey 2003;

† Email address for correspondence: s.kalliadasis@imperial.ac.uk

Callies & Quéré 2005) as well as recent advances in substrate fabrication techniques that have enabled the control of substrate features down to the micro-scale (Bico, Tordeux & Quéré 2001). We note that in all these studies the topography is well-defined/structured consisting of regular micro-scale features, e.g. pillars ('textured substrates').

The first study on contact line equilibria over rough substrates was conducted by Wenzel (1936). He utilized energetic/thermodynamic arguments to obtain an effective apparent contact angle, θ_r:

$$\cos\theta_r = r\cos\alpha_s, \tag{1.1}$$

where α_s is the static contact angle and r is the roughness coefficient of the substrate, corresponding to the ratio of the real to the projected area of the substrate. This coefficient is introduced phenomenologically and without any explicit reference to the topography shape. McHale (2007) proposed the use of a spatially varying roughness coefficient to allow for substrates whose features are not isotropically distributed, as for example substrates with a single defect or when the features are arranged with an identifiable orientation that would perhaps favour spreading in a specific direction. Since $r > 1$ always, when $\alpha_s < \pi/2$ we find that $\theta_r < \alpha_s$, which then suggests that substrate roughness always enhances wetting. Despite the fact that a number of experimental studies appear to confirm approximately Wenzel's formula (see for example Hitchcock, Carroll & Nicholas 1981; Shibuichi *et al.* 1996; Bico *et al.* 2001), its generality is questionable as a result of the simplicity of the arguments leading to its derivation which do not reflect the actual complexity of wetting in the presence of topography. Indeed, the experiments by Oliver, Huh & Mason (1977) and more recently the work by Chung, Youngblood & Stafford (2007) with a droplet spreading on parallel-grooved substrates suggest that, contrary to the predictions of (1.1), wetting inhibition instead of enhancement is possible when spreading normal to the substrate grooves.

The few theoretical studies on the problem of the statics of contact lines over topographical substrates focused mainly on deterministic substrates. For example, Johnson & Dettre (1964) studied the effect of roughness on the wettability of substrates with axisymmetric, periodic grooves by using energetic/thermodynamic arguments. Their analysis suggested that multiple metastable configurations exist that are separated by energy barriers, while the lowest energy of these metastable states corresponds to the equilibrium predicted by (1.1). Huh & Mason (1977) adopted a purely fluid mechanics approach and also worked with axisymmetric, periodic substrates. They found that contact angle hysteresis may be attributed to the multiple equilibria. They also postulated that upon changing the droplet volume, the contact line would exhibit a stick-jump behaviour, which was observed experimentally in a subsequent study (Oliver, Huh & Mason 1980), but not in a reproducible manner that would allow direct comparisons with their theory. Furthermore, they offered a brief discussion on random substrates and suggested that hysteresis may be attributed to the randomness of the substrate. Cox (1983) examined multiple equilibria of an infinite fluid wedge on a general non-periodic rough substrate and concluded that hysteresis in the apparent contact angle can be attributed, at least in part, to substrate roughness, thus offering corroborating theoretical evidence to the above statement by Huh & Mason (1977) on random substrates.

Introducing randomness in the substrate variations is clearly a more realistic way to represent roughness. There are very few studies in this direction, but did not quantify the effects of roughness in a systematic manner. For example, Palasantzas

& De Hosson (2001), generalizing the earlier work of Zhou & De Hosson (1995), attempted to distinguish between the angles deduced from the fluid mechanics and the thermodynamic approaches (i.e. Wenzel's relation; see for example Good 1952; Hazlett 1992) by postulating, without formal justification, an effective contact angle related to the harmonic mean of the squares of these angles. Hazlett (1990) proposed a modified version of Wenzel's equation based on thermodynamics by assuming substrates with a fractal structure that persists for all scales. This is clearly not realistic, and also such structures could not be used in a fluid mechanics study due to the difficulty in uniquely prescribing a normal vector to a function that is nowhere differentiable. Other studies were based on phenomenological modelling ideas and postulated equations, as for example the study by Jansons (1985), who regarded rough substrate patches as contact angle point sources, or the one by Borgs *et al.* (1995), who examined the effects of surface roughness by using an Ising model. Finally, the work of Robbins & Joanny (1987), which is essentially an extension of the previous studies by Joanny & de Gennes (1984) and Pomeau & Vannimenus (1985) to random heterogeneities, examined the origin of contact angle hysteresis based on the assumption that both chemical and topographical heterogeneities are completely analogous to each other and, through energetic arguments, they examined the contact line equilibria of a wedged fluid mass to quantify hysteresis via scaling laws expressed in terms of a pinning force.

Hence, a systematic fluid mechanics treatment of the statics of contact lines based on statistical approaches is presently lacking. In Part 1 of this two-part study, we present a theoretical framework for studying the influence of substrate roughness on contact lines by developing appropriate statistical methodologies. Our model system consists of a two-dimensional droplet, referred to hereafter simply as 'droplet', on a spatially heterogeneous substrate modelled as a random function. The main aim is to investigate theoretically the effects of such heterogeneities on the contact lines. Our focus here is the droplet equilibria while in Savva, Pavliotis & Kalliadasis (2010, hereafter referred to as Part 2), we examine the spreading dynamics of the droplet. Of course, by restricting our attention to two dimensions we avoid some of the intricacies of a three-dimensional setting, e.g. dealing with a two-dimensional contact line. The restriction to a two-dimensional configuration simplifies the problem considerably, but nevertheless, the analysis is already highly non-trivial. Also, we believe that despite the assumption of two-dimensionality, our study captures the basic physics and several of the qualitative features of the effects of roughness on contact lines.

We begin in § 2 with the development of an appropriate stochastic representation of the spatial heterogeneities, which both facilitates the analysis and can satisfactorily represent an actual substrate. This is taken to be a band-limited white noise. Assuming shallow and slowly varying topographies, we deduce in § 3 the equations governing droplet equilibria. They can be substantially simplified via a linearization about the ideally flat-substrate case equilibrium. This leads to a system of equations for the contact line fluctuation and droplet shift along the substrate. The statistics of the droplet shift is analysed in § 4 both for weakly and fully asymmetric substrates; due to the complexity of the equations, it can only be determined approximately. In § 5 we examine the statistics of the droplet radius, which is found to be a normally distributed random variable whose variance increases with substrate roughness. Our theoretical predictions are verified with numerical experiments. In § 6 we offer a generalization to arbitrary stationary random functions. For specific substrate models, we deduce expressions for the variance of the contact line fluctuation and we demonstrate that its statistics do not differ qualitatively from those obtained for the band-limited

white-noise representation used throughout the previous sections. A concluding discussion is given in § 7.

2. Substrate representation

The first fundamental question for the problem of a contact line on a random substrate is the development of an appropriate stochastic representation of the substrate. For this purpose we invoke a random-function representation, first proposed by Whitehouse & Archard (1970) to study problems pertaining to surface contact. To avoid ambiguity in the definition of contact angles near sharp substrate edges, continuity of the substrate profile and its derivatives is essential. Furthermore, in addition to specifying a characteristic amplitude, it is also desirable to be able to have a broad and controllable frequency content. Hence, the substrate profile, prescribed by $\eta(x)$, can be most conveniently represented as the following random function,

$$\eta(x) = \frac{\eta_0}{\sqrt{N}} \sum_{m=1}^{N} \left[\alpha_m \sin\left(\frac{k_0 m}{N} x\right) + \beta_m \cos\left(\frac{k_0 m}{N} x\right) \right], \tag{2.1}$$

where η_0 and k_0 are the characteristic amplitude and wavenumber of the substrate, respectively, and N is a large positive integer. The coefficients α_m, β_m are independent, Gaussian random variables with $\langle \alpha_m^2 \rangle = \langle \beta_m^2 \rangle = 1$, where $\langle \cdot \rangle$ is used to denote the ensemble average over all possible realizations of $\eta(x)$. The above expression is introduced with the understanding that, technically speaking, α_m and β_m should be written as functions of some parameter, say ω, which belongs to the space of random events (i.e. substrate realizations), Ω. Nevertheless, ω is suppressed throughout for simplicity of notation.

Figure 1 depicts sample substrate realizations for different k_0 and fixed $\eta_0 = 10^{-3}$ and $N = 1000$. Evidently, $\eta(x)$ becomes highly oscillatory as k_0 increases. It is readily seen that $\eta(x)$ is a periodic function with period $2\pi N/k_0$, but we eventually take $N \to \infty$ so that this periodicity is lost. As shown in the Appendix, continuity of all realizations of $\eta(x)$ and their derivatives follows directly from Kolmogorov's continuity theorem (Øksendal 2003), provided that k_0 is finite.

This substrate representation implies that for fixed x, $\eta(x)$ is also a Gaussian variable. However, the Gaussianity of the substrate is not postulated just for the sake of mathematical convenience; it is also demonstrated in a number of studies with actual rough substrates (see e.g. Greenwood & Williamson 1966). For substrates which are not normally distributed, predictions for the substrate statistics obtained with the Gaussian assumption are found to be in good agreement with experiments (Thomas 1999, and references therein). Furthermore, in the following we shall utilize the long-wave approximation to obtain a simple model for the droplet equilibria. We then assume a shallow and slowly varying substrate. This is actually a realistic assumption for a broad range of substrates, since, as pointed out by Thomas (1999), substrate slopes are usually quite gentle, at least within the resolution of the instruments. This may be contrary to what one would expect: the variations of the substrate are often thought to occur at small wavelengths compared with the substrate height. This is a common misconception in substrate profilometry that stems from the way an experimental profile is presented with the tendency to overly exaggerate the vertical magnification over the horizontal one (see figure 2).

The random function chosen to represent the substrate (2.1) is stationary. Stationary random functions are characterized by the property that the correlation of the

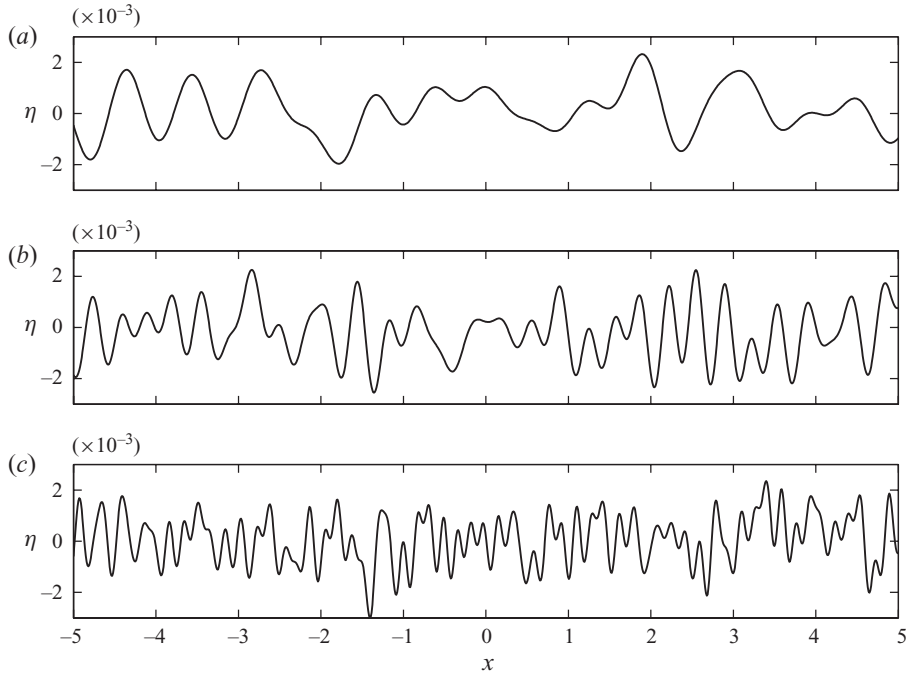

FIGURE 1. Sample substrate realizations using $\eta_0 = 10^{-3}$ with (*a*) $k_0 = 10$, (*b*) $k_0 = 20$ and (*c*) $k_0 = 40$.

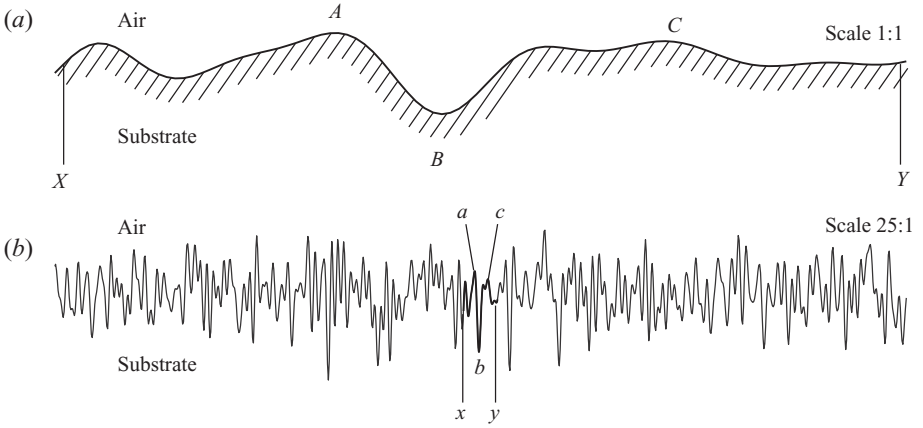

FIGURE 2. Effect of horizontal compression of profile measurements: (*a*) actual appearance of section XY; (*b*) compressed representation. Lower-case letters correspond to the upper case letters of (*a*).

amplitudes at two different locations, x_1 and x_2, is a function of $x_1 - x_2$ only, i.e.

$$\langle \eta(x_1)\,\eta(x_2)\rangle = \frac{\eta_0^2}{N}\sum_{m=1}^{N}\cos\left(\frac{k_0 m}{N}(x_1 - x_2)\right) = \eta_0^2\,\mathrm{sinc}\left[k_0(x_1 - x_2)\right], \qquad (2.2)$$

where $\mathrm{sinc}\,x = x^{-1}\sin x$ is the cardinal sine function. Here the last equality is taken with the understanding that we take the limit $N \to \infty$, which allows us to essentially

convert the Riemann sum into an integral. Such manipulations are commonly used throughout both parts of the study to evaluate the limiting behaviours of these sums. Even though the assumption of substrate stationarity is open to controversy (see e.g. Sayles & Thomas 1978; Mulvaney, Newland & Gill 1989; Whitehouse 2001, and the references therein), with researchers who either favour it or oppose it, we will proceed with this assumption in order to make progress in our problem theoretically. We shall nevertheless elaborate more on this and related issues in § 6, where we generalize our analysis to arbitrary stationary random functions with normally distributed height, imposing however the necessary cutoffs to ensure conformity with our assumptions of continuity and differentiability.

A particularly attractive feature of this representation is that each substrate family depends on two parameters only, η_0 and k_0, which are often reported in experimental studies when characterizing a rough substrate (e.g. Hitchcock *et al.* 1981). In an experiment, η_0 can be estimated from $\eta_0 = \sqrt{\mathrm{Var}[\eta]}$, whereas k_0 can be determined from

$$k_0 = 2\pi n\sqrt{\frac{5}{3}}, \tag{2.3}$$

where n is the number of substrate maxima per unit length. Equation (2.3) was deduced by Rice (1945) by considering the joint probability density function of η, η' and η'', where the primes denote differentiation with respect to x, and finding the probability that η' vanishes for some fixed x while $\eta'' < 0$. These two parameters can also be used to compute the roughness coefficient of the substrate, r, defined as the mean ratio of the actual surface area over its projected area as we first noted in § 1:

$$r = \left\langle \frac{\text{Actual 'area'}}{\text{Projected 'area'}} \right\rangle = \left\langle \frac{k_0}{2\pi N} \int_{-\pi N/k_0}^{+\pi N/k_0} \sqrt{1 + [\eta'(x)]^2}\, \mathrm{d}x \right\rangle. \tag{2.4}$$

In the limit $\eta_0 k_0 \ll 1$, we find

$$r \approx \left\langle \frac{k_0}{2\pi N} \int_{-\pi N/k_0}^{+\pi N/k_0} \left(1 + \frac{1}{2}\left[\eta'(x)\right]^2\right) \mathrm{d}x \right\rangle = 1 + \frac{1}{6}\eta_0^2 k_0^2, \tag{2.5}$$

which may be contrasted with $1 + \eta_0^2 k_0^2/4$ obtained for a pure harmonic such as $\eta(x) = \eta_0 \cos k_0 x$ (de Gennes, Brochard-Wyart & Quéré 2003). Another measure for substrate roughness is the roughness or Hurst exponent, ζ, defined by the asymptotic behaviour of $\langle[\eta(x_1) - \eta(x_2)]^2\rangle^{1/2} \sim |x_1 - x_2|^{\zeta}$ when $|x_1 - x_2| \to \infty$ (Barabási & Stanley 1995). For (2.1), $\zeta = 0$. The roughness exponent typically varies between 0 and 1 and, as we shall see in § 6, it can be viewed as a measure of the self-similarity and the correlation properties of the substrate features.

In the limit $N \to \infty$ and for finite k_0, (2.1) represents band-limited white noise, meaning that all wavenumbers in the interval $[0, k_0]$ are equally probable to be present; all other wavenumbers have zero probability of occurring. Representations of this form are also invoked to look into noise effects in other contexts, for example, in electrical current signals or in black-body radiation (Rice 1945). In the context of electrical signals, our representation is analogous to a signal going through a low-pass filter that attenuates all frequencies larger than $k_0/(2\pi)$.

Admittedly, (2.1) may be regarded as a simplistic representation of a realistic rough substrate, especially because other substrate representations could have been chosen which compare well with experimental substrate profiles (see e.g. Sayles & Thomas 1978; Mulvaney *et al.* 1989; Bhushan & Majumdar 1992). However, such representations typically require more parameters than the one suggested here. And, as

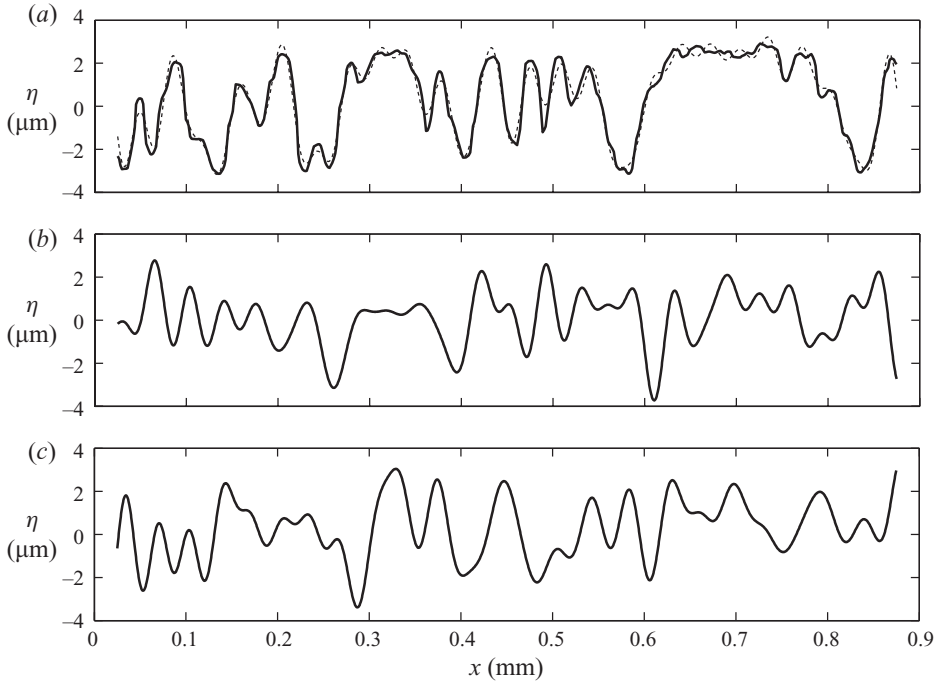

FIGURE 3. (*a*) Comparison of the experimentally measured substrate profile by Hitchcock *et al.* (1981) (solid line) with an approximation generated using (2.1) (dashed line), where k_0 is found from (2.3); (*b*, *c*) substrate realizations using the parameters η_0 and k_0 determined from the experimental profile of (*a*).

pointed out earlier, usually η_0 and k_0 are the only parameters reported in experimental studies characterizing rough substrates and (2.1) is the simplest representation that is completely described by these two parameters. At the same time, a comparison with scanning-electron microscopy images by Hitchcock *et al.* (1981) suggests that (2.1) may be used to adequately represent a real substrate. In figure 3(*a*) we use the expansion in (2.1) to approximate a substrate profile taken from the work of Hitchcock *et al.* (1981), by determining k_0 and η_0 from (2.3) and the amplitude variance, respectively, and obtaining the respective α_m and β_m by appropriately projecting a fixed number of harmonics onto the substrate profile. Using the same η_0 and k_0 obtained from (2.3), sample substrate profiles are generated in figure 3(*b*, *c*) with random α_m and β_m and $N = 1000$ for a visual comparison of the experimentally measured profile and random members of the same substrate family.

It is noteworthy that the use of other substrate representations that comply with our requirements of continuity and differentiability is not expected to alter the equilibrium statistics dramatically. Indeed, as we shall demonstrate in § 6, the statistical properties of substrates with both exponentially decaying correlations (Whitehouse & Archard 1970) and power-law correlations, known to produce fractal structures that do not persist for all scales (Sayles & Thomas 1978), differ only by a prefactor from the leading-order statistics obtained from (2.1) to represent a family of substrates. This prefactor is naturally dependent on the extra parameters that are introduced to describe these more sophisticated models. Moreover, given also the uncertainty associated with the measuring instruments in general, we believe

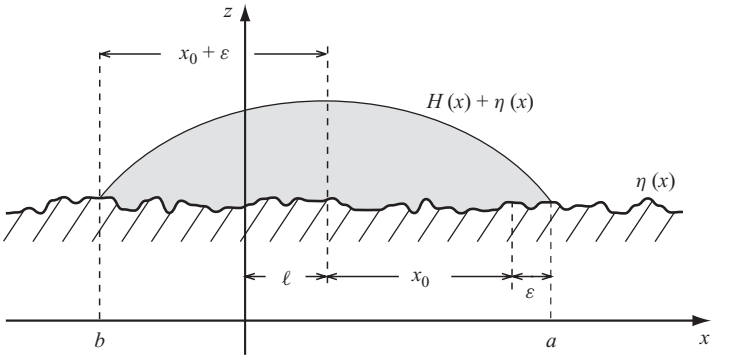

FIGURE 4. Droplet on a random topographical substrate and in the domain $b \leqslant x \leqslant a$. The droplet shift defined as $\ell = (a+b)/2$ is the distance the droplet midpoint is shifted away from $x = 0$, and the contact line fluctuation defined as $\varepsilon = (a-b)/2 - x_0$ measures deviations of the contact line location away from the flat-substrate radius, $x_0 = \sqrt{3}$.

that these differences are of secondary importance compared to our principal aim to investigate the qualitative effects of substrate topography on contact lines.

3. Equations for droplet equilibria

Consider a droplet of thickness $H(x)$ on the x–z plane resting on a substrate whose profile $z = \eta(x)$ is prescribed by (2.1) (see figure 4). Our starting point is the classical Young–Laplace equation

$$\frac{(H+\eta)''}{[1+(H+\eta)'^2]^{3/2}} = \frac{\Delta p}{\sigma}, \tag{3.1}$$

where Δp is the constant pressure difference across the droplet interface and σ is the air–liquid surface tension. Assuming that the static contact angle, α_s, is small and that the substrate variations are slow, we may neglect $(H+\eta)' \ll 1$, so that the governing equation becomes

$$(H+\eta)''' = 0, \tag{3.2}$$

upon differentiation with respect to x. Equation (3.2) is cast in non-dimensional form by scaling x with L and $H(x)$ and $\eta(x)$ with $L\tan\alpha_s$, where the length scale L is defined as $L = \sqrt{A/(2\tan\alpha_s)}$ and A is the cross-sectional area of the droplet profile. Assuming that the droplet lies in the interval $b \leqslant x \leqslant a$, (3.2) is subject to a constant-area constraint, $\int_b^a H(x)\,\mathrm{d}x = 2$, and the boundary condition $H(a) = H(b) = 0$ at the two contact points to obtain the droplet thickness

$$H(x) = \frac{6}{(a-b)^3}\left[2 + \int_b^a \eta(x)\,\mathrm{d}x - \frac{1}{2}(\eta_a + \eta_b)(a-b)\right][(a+b)x - x^2 - ab] + \eta_a\frac{x-b}{a-b} + \eta_b\frac{a-x}{a-b} - \eta(x), \tag{3.3}$$

where $\eta_a = \eta(a)$, $\eta_b = \eta(b)$, $\eta_a' = \eta'(a)$ and $\eta_b' = \eta(b)$.

The (yet unknown) contact line locations, a and b, are determined by requiring the droplet to meet the substrate at an angle equal to α_s, using $H'(a) = -\tan\theta_a$ and

$H'(b) = \tan\theta_b$, where $\tan\theta_{a,b}$ are expressed in terms of $\tan\alpha_s$, $\eta'(a)$ and $\eta'(b)$:

$$\tan\theta_a = \frac{1+\tan\alpha_s^2\eta'^2_a}{1+\tan\alpha_s^2\eta'_a} \quad \text{and} \quad \tan\theta_b = \frac{1+\tan\alpha_s^2\eta'^2_b}{1-\tan\alpha_s^2\eta'_b}, \tag{3.4}$$

derived in Savva & Kalliadasis (2009) from simple geometric considerations and a straightforward application of the tangent summation and subtraction identities. The long-wave approximation is invoked to simplify the contact-angle conditions with $\tan\theta_{a,b} \approx 1$, so that the contributions of the topography to the derivatives of H at the contact points are neglected. The contact line locations are found by solving the system of equations that correspond to $H'(b) - H'(a) = 2$ and $H'(a) + H'(b) = 0$, respectively,

$$(\eta'_a - \eta'_b - 2)(a-b)^2 - 6(\eta_a+\eta_b)(a-b) + 12\int_b^a \eta(x)\,\mathrm{d}x + 24 = 0, \tag{3.5a}$$

$$(\eta'_a + \eta'_b)(a-b) = 2(\eta_a - \eta_b). \tag{3.5b}$$

The analysis is facilitated if we let

$$a = \ell + d \quad \text{and} \quad b = \ell - d, \tag{3.6}$$

where d and ℓ are the droplet radius and *droplet shift* corresponding to the displacement of the droplet midpoint away from $x = 0$, respectively (see figure 4). The above change of variables together with (2.1) transform (3.5) to

$$d - \frac{3}{d} = \frac{\eta_0}{\sqrt{N}}\sum_{m=1}^{N}(\alpha_m \sin k_m\ell + \beta_m \cos k_m\ell)\,F(k_m d), \tag{3.7a}$$

$$0 = \sum_{m=1}^{N}(\alpha_m \cos k_m\ell - \beta_m \sin k_m\ell)\,G(k_m d), \tag{3.7b}$$

where $k_m = k_0 m/N$ and

$$F(x) = 3\,\mathrm{sinc}\,x - 3\cos x - x\sin x, \tag{3.8}$$

$$G(x) = x\cos x - \sin x. \tag{3.9}$$

For $\eta(x)$, we use (2.1) and since we are interested in small-scale roughness, we take $\eta_0 \ll 1$ and further assume that $\eta_0 k_0 \ll 1$ to conform with our original assumption of slow substrate variations. Solutions to the nonlinear system of equations (3.7) are obtained perturbatively up to $O(\eta_0^2)$ using the expansion about the flat-substrate equilibria,

$$d = \sqrt{3} + \varepsilon, \tag{3.10}$$

where ε is the *contact line fluctuation*, a measure of the deviation of the droplet radius from the flat-substrate case. In the absence of the topography, $d = \sqrt{3}$, and ℓ is arbitrary due to the translational invariance along the substrate. In the presence of topography, this invariance is broken, ℓ is no longer arbitrary and we need to solve the system of equations (3.7) for d and ℓ. It is clear that provided $\eta_0 \ll 1$, $\varepsilon = O(\eta_0)$. The droplet shift however can be of any order, so we cannot generally assume that it is small. Substituting (3.10) in (3.7*a*) and linearizing yields

$$\varepsilon = \frac{\eta_0}{2\sqrt{N}}\sum_{m=1}^{N}(\alpha_m \sin k_m\ell + \beta_m \cos k_m\ell)\,F(k_m\sqrt{3}) + O\left(\eta_0^2, \eta_0^2 k_0, \eta_0^2 k_0^2\right). \tag{3.11}$$

This expansion is valid provided that the neglected terms are small, i.e. when

$$\eta_0 k_0^2 \ll 1. \tag{3.12}$$

Likewise, linearization of (3.7*b*) using (3.10) gives

$$\sum_{m=1}^{N} (\alpha_m \cos k_m \ell - \beta_m \sin k_m \ell) \left[G(k_m \sqrt{3}) + O\left(\eta_0 k_0^2\right) \right] = 0, \tag{3.13}$$

where the higher-order correction is neglected in accord with (3.12).

Equations (3.11) and (3.13) describe, to leading order in η_0, the equilibrium contact line locations for a particular realization of α_m and β_m. Knowing the precise form of a substrate with such small asperities is impractical however, whereas a statistical approach, described in more detail in the following sections, is more appropriate in order to assess their effect on the equilibria.

Given that our principal aim is to look into the effects of small-scale roughness, we would like to have k_0 as large as possible. To proceed with the present analysis, however, it is also necessary to conform with the above condition and for this reason we will investigate substrate families with $\eta_0 \ll 1$ and $1 \ll k_0 \ll \eta_0^{-1/2}$. Hence, for a droplet with $L = 0.5$ mm, $\alpha_s = 15^\circ$ and a substrate topography with characteristic amplitude 0.5 μm ($\eta_0 \approx 4 \times 10^{-4}$), $\eta_0 k_0^2 < 1$ for wavelengths longer than 77 μm. Roughness at such scales can be found in a range of actual substrates (see e.g. Hitchcock *et al.* 1981).

4. Droplet shift statistics

When the amplitude of the topography is small, we see from (3.13) that ℓ does not depend on η_0, to leading order in η_0. Equation (3.13) also suggests that there may exist infinitely many solutions for ℓ. When a single wavenumber, k_0, is present, these equilibria correspond to infinite identical equilibrium droplet shapes separated by a distance $\Delta\ell = 2\pi/k_0$ due to the inherent substrate periodicity. In our description, however, there exists a continuum of wavenumbers and an analytical solution to (3.13) cannot be found. Hence, to be able to quantify the statistics of ℓ, we seek a solution that is closest to $\ell = 0$. Despite the fact that for each substrate realization there corresponds a unique solution for ℓ, there is no reason for the droplet equilibrium to favour being shifted, on average, either left or right and hence, by symmetry, we expect that $\langle \ell \rangle = 0$. Moreover, since the choice of the origin is arbitrary in this setting, the problem is essentially equivalent to finding the equilibrium nearest to the flat-substrate equilibrium, $a = -b = \sqrt{3}$. Even with this restriction, ℓ need not be small and hence a perturbative approach is not generally applicable.

4.1. *Weakly symmetric substrates*

A perturbative solution to the equations can be nevertheless obtained for substrates that exhibit weak asymmetry with respect to our chosen origin, i.e. by replacing α_m with $\delta\alpha_m$, where $\delta \ll 1$ is assumed to be a small constant. By doing so, the substrate becomes non-stationary, since $\langle \eta(x_1)\eta(x_2) \rangle$ is no longer a function of $x_1 - x_2$ only, but now we can simplify (3.13) as

$$\sum_{m=1}^{N} (\delta\alpha_m - \beta_m k_m \ell)\, G(k_m \sqrt{3}) + O\left(\delta^2 k_0^2\right) = 0. \tag{4.1}$$

The neglected terms are indeed negligible provided that $\delta \ll k_0^{-1}$. Solving (4.1) for ℓ gives

$$\ell = \frac{\delta \sum_{m=1}^{N} \alpha_m G(k_m \sqrt{3})}{\sum_{m=1}^{N} \beta_m k_m G(k_m \sqrt{3})}. \tag{4.2}$$

Hence, we see that (4.2) is expressed as a ratio of two random variables

$$X_1 = \frac{\delta}{\sqrt{N}} \sum_{m=1}^{N} \alpha_m G(k_m \sqrt{3}) \quad \text{and} \quad X_2 = \frac{1}{\sqrt{N}} \sum_{m=1}^{N} \beta_m k_m G(k_m \sqrt{3}), \tag{4.3}$$

which are independent, zero-mean normal variables with variances

$$\sigma_1^2 = \delta^2 \int_0^1 [G(k_0 y \sqrt{3})]^2 \, \mathrm{d}y \quad \text{and} \quad \sigma_2^2 = k_0^2 \int_0^1 [y G(k_0 y \sqrt{3})]^2 \, \mathrm{d}y, \tag{4.4}$$

respectively. From probability theory, ℓ is a Cauchy random variable (Geary 1930) with the scale parameter $\xi = \sigma_1/\sigma_2$, which corresponds to the distance for which the probability that ℓ lies between $-\xi$ and $+\xi$ is 1/2. In the limit of $k_0 \gg 1$, the asymptotic form of ξ is

$$\xi^2 \sim \frac{5\delta^2}{3k_0^2}[1 - 2\,\mathrm{sinc}(2k_0\sqrt{3})] + O\left(k_0^{-4}\right). \tag{4.5}$$

Cauchy random variables are encountered in a variety of different contexts in physics (see e.g. Krishnamoorthy 2006, and the references therein) and their probability density function is given by

$$p_\ell(\ell) = \frac{1}{\pi} \frac{\xi}{\ell^2 + \xi^2}. \tag{4.6}$$

For Cauchy random variables, it is known that neither the mean nor the variance of ℓ is defined. As k_0 increases, it is expected to obtain narrower probability densities, meaning that more droplet equilibria can be found that are close to $\ell = 0$. However, the relatively flat tails of the probability density suggest that it is not uncommon to find an equilibrium that is far from $\ell = 0$.

To confirm the above calculation, we compute the statistics of 2×10^4 substrate realizations for families with $\eta_0 = 10^{-3}$ and $k_0 = 10$, 20 and 40, using $\delta = 0.01$. The same set of numerical experiments is repeated for $\delta = 0.05$. In figures 5(a) and 5(b) we show plots of the experimentally determined probability densities for $\delta = 0.01$ and $\delta = 0.05$, respectively, together with their respective probability densities predicted by theory (4.6). Apart from the excellent agreement between theory and experiment, we also confirm the self-similarity of the density with respect to the length scale ξ, which depends linearly on δ for fixed k_0. This explains why when $\delta = 0.01$, p_ℓ is 5 times taller and 5 times narrower compared to the densities when $\delta = 0.05$.

4.2. *Fully asymmetric substrates*

In reality however, it is difficult to encounter a random substrate that is symmetric or nearly symmetric. Despite the fact that we can no longer solve explicitly for ℓ, we would like to characterize its statistics for the general case of families of asymmetric substrates. Seeking ℓ that is closest to $\ell = 0$ is reminiscent of the 'first-passage problem' in probability theory, which is often encountered in stochastic

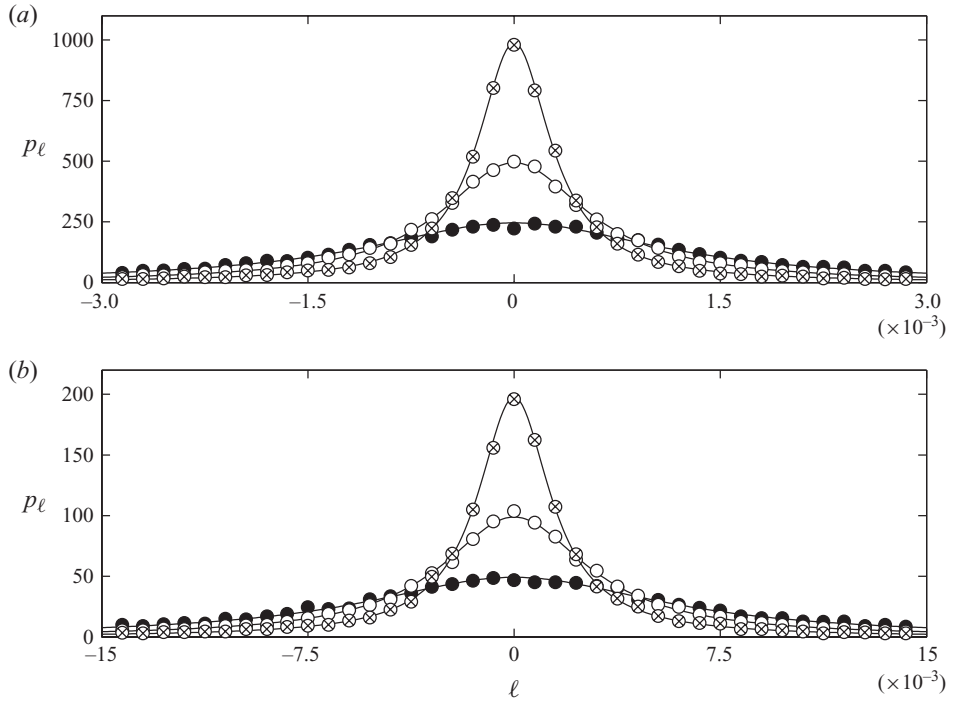

FIGURE 5. Probability density function of ℓ determined from numerical experiments using 2×10^4 substrate realizations with $\eta_0 = 10^{-3}$ and $k_0 = 10\,(\bullet)$, $20\,(\circ)$ and $40\,(\otimes)$ with (a) $\delta = 0.01$ and (b) $\delta = 0.05$. The solid line shows the corresponding probability densities predicted by theory (4.6). As k_0 increases, the probability density functions become narrow and taller, illustrating the fact that more and more droplet equilibria can be found closer to $\ell = 0$.

dynamical systems when it is desirable to know the probability distribution of the first time a stochastic process attains a specified value (van Kampen 2007). First-passage problems are usually associated with a time variable, but the theory readily applies in this context as well; instead of finding the statistics of the first time a random process goes through a zero, we seek the statistics of the equilibrium that is closest to the origin, given by the zero of a Gaussian random field, i.e. the left-hand side of (3.13). This equivalence is made more transparent, if one considers separately sample paths/realizations of, say, a time-dependent random process and a realization of (3.13), which is space-dependent. In first-passage analysis, the first time that each realization of the random process goes through a zero is taken into account, whereas in our analysis we seek the zero of each realization of (3.13) which is closest to the origin, $\ell = 0$. Consequently, the mathematical problem is essentially the same, the only difference being that we replace time with space, in a way that also allows us to take into account equilibria that are both to the left and right of the origin.

First-passage problems find applications in a variety of contexts in science and engineering ranging from chemistry and signal transmission theory to ocean science and to certain interface de-pinning problems (see e.g. Zeitak 1997; Roberts & Torquato 1999, and the references therein). Even though Rice (1945) provided a formal series solution to the problem of finding the probability density function for the first-passage time for Gaussian processes, his formalism involved evaluations of integrals that became increasingly difficult to compute for each successive term in this series.

Other authors proposed different approaches (see e.g. Longuet-Higgins 1958), but to date this problem has not yet been fully resolved analytically.

From the above discussion, obtaining the probability density function of ℓ is not analytically tractable, but a hybrid analytical/numerical approach is possible. The key to this approach is to recognize that in the class of problems we consider, there is an intrinsic length scale given by the mean distance between zeros of (3.13), $\langle \Delta\ell \rangle$. This may be directly deduced from the work of Rice (1945), who obtained the mean number of zero crossings per unit length of a stationary Gaussian random process, $\langle \Delta\ell \rangle$, where

$$\langle \Delta\ell \rangle = \frac{\pi}{k_0} \sqrt{\frac{\displaystyle\int_0^1 [G(k_0 y\sqrt{3})]^2 \,\mathrm{d}y}{\displaystyle\int_0^1 [yG(k_0 y\sqrt{3})]^2 \,\mathrm{d}y}}, \tag{4.7}$$

which, coincidentally, is identical to ξ in (4.5) when $\delta = \pi$. By symmetry, we can argue that on average the last negative and first positive root of (3.13) lies at a distance $\langle \Delta\ell \rangle/2$ from the origin. Hence, for the variance of ℓ, $\mathrm{Var}[\ell]$, we expect that

$$\mathrm{Var}[\ell] = \frac{1}{2}\left(\frac{\langle \Delta\ell \rangle}{2}\right)^2 \sim \frac{5\pi^2}{24k_0^2}[1 - 2\,\mathrm{sinc}(2k_0\sqrt{3})] + O\left(k_0^{-4}\right) \tag{4.8}$$

in the limit of $k_0 \gg 1$. This implies that as the characteristic length scale of substrate variations becomes shorter, the droplet slides/shifts less to find a nearby equilibrium. Apart from the variance and mean of ℓ, we can gain additional information for the Taylor expansion of the probability density of ℓ, p_ℓ, about $\ell = 0$ using the work of Zeitak (1997) on the early-time expansion of first-passage distributions. In particular, for a stationary Gaussian process $W(\ell)$ with correlation function

$$C(\ell) = \langle W(l+\ell)\, W(l) \rangle = 1 + c_2\ell^2 + c_4\ell^4 + c_6\ell^6 + O(\ell^8), \tag{4.9}$$

Zeitak (1997) considered the probability that $W(\ell)$ does not change sign in $[0, \ell]$, which is equivalent to requiring that the extrema of $W(\ell)$ are of the same sign as $W(0)$, eventually showing that the probability density of the first-passage problem has the following Taylor expansion about $\ell = 0$:

$$p_\ell = \frac{\sqrt{-2c_2}}{\pi} - \frac{6c_4 - c_2^2}{4\pi\sqrt{-2c_2}}\ell^2 - \frac{43c_2^4 - 260c_2^2c_4 - 20c_4^2 + 80c_2c_6}{32c_2\pi\sqrt{-2c_2}}\ell^4 + O(\ell^6). \tag{4.10}$$

Thus, to be able to fully resolve the behaviour of p_ℓ, we need to compute c_2, c_4 and c_6 of a properly defined random function $W(\ell)$. Hence, using (3.13) we define

$$W(\ell) = \frac{1}{\sqrt{N}\displaystyle\int_0^1 [G(k_0 y\sqrt{3})]^2 \,\mathrm{d}y} \sum_{m=1}^{N} (\alpha_m \cos k_m\ell - \beta_m \sin k_m\ell)\, G(k_m\sqrt{3}), \tag{4.11}$$

which has the following correlation function:

$$C(\ell) = \frac{\displaystyle\int_0^1 \cos(yk_0\ell) G(k_0\sqrt{3}y)^2 \,\mathrm{d}y}{\displaystyle\int_0^1 [G(k_0 y\sqrt{3})]^2 \,\mathrm{d}y}, \tag{4.12}$$

upon conversion of the Riemann sum to an integral. Expanding (4.12) for small ℓ and matching powers of ℓ with (4.9) we find that

$$c_2 = -\frac{\pi^2}{2\langle\Delta\ell\rangle^2} \quad \text{and} \quad c_{2j} = (-1)^{j+1}\frac{k_0^{2j}\displaystyle\int_0^1 y^{2j}G(k_0\sqrt{3}y)^2\,\mathrm{d}y}{(2j)!\displaystyle\int_0^1 [G(k_0y\sqrt{3})]^2\,\mathrm{d}y}, \quad j = 2,\ 3. \tag{4.13}$$

Again, since we are interested in the limit of $k_0 \gg 1$, the asymptotic form of the first three terms in the expansion for p_ℓ, (4.10) becomes

$$\left.\begin{aligned} p_{\ell 0} &= \frac{\sqrt{-2c_2}}{\pi} = \frac{1}{\langle\Delta\ell\rangle} \sim \frac{k_0}{2\pi}\sqrt{\frac{3}{5}}\left[1 + \operatorname{sinc}(2k_0\sqrt{3}) + O\left(k_0^{-2}\right)\right], \\ p_{\ell 2} &= \frac{6c_4 - c_2^2}{4\pi\sqrt{-2c_2}} \sim \frac{k_0^3}{140\pi}\sqrt{\frac{3}{5}}\left[1 + 3\operatorname{sinc}(2k_0\sqrt{3}) + O\left(k_0^{-2}\right)\right], \\ p_{\ell 4} &= \frac{43c_2^4 - 260c_2^2c_4 - 20c_4^2 + 80c_2c_6}{32c_2\pi\sqrt{-2c_2}} \\ &\sim \frac{17867k_0^5}{7938000\pi}\sqrt{\frac{3}{5}}\left[1 + 5\operatorname{sinc}(2k_0\sqrt{3}) + O\left(k_0^{-2}\right)\right]. \end{aligned}\right\} \tag{4.14}$$

Now that we have some information about p_ℓ, we can construct an approximation to it via a Padé approximant (Baker & Graves-Morris 1996). This is most conveniently done with

$$p_\ell^{\text{Padé}} = \frac{p_{\ell 0}^3}{q\ell^6 + \left(p_{\ell 4}p_{\ell 0} + p_{\ell 2}^2\right)\ell^4 + p_{\ell 0}p_{\ell 2}\ell^2 + p_{\ell 0}^2}, \tag{4.15}$$

which automatically satisfies (4.10) for small ℓ and the unknown q is found from the normalization constraint for p_ℓ. A Padé approximant of this form guarantees decay to zero as $\ell \to \infty$, and in all of the numerical experiments considered the denominator had no poles on the real line; we thus obtain an everywhere-continuous approximation to the probability density of ℓ. Even though a higher-degree polynomial could have been used in the denominator so that the variance of ℓ could also be incorporated in obtaining an approximant, it was generally hard to find an approximant that was positive for all ℓ.

In figure 6(*a*) we show the Padé approximant obtained when $k_0 = 10$, together with the corresponding probability densities obtained in numerical experiments with $\eta_0 = 5\times10^{-4}$, 10^{-3}, 5×10^{-3} and 10^{-2}, utilizing 2×10^4 substrate realizations from each family. This plot demonstrates the independence of p_ℓ on η_0. We note that ℓ is far from being a normally distributed normal variable upon comparison with the equivalent normal density depicted with the dashed line. We also note that the Padé approximant satisfactorily predicts the probability densities for all amplitudes, even for substrate families that lie beyond the regime of validity of our perturbation procedure (3.12). This agreement however is not expected to persist as the substrates become more 'rough'. Indeed, when the same set of calculations was repeated for $k_0 = 20$, the agreement with the approximant is found to be dependent on η_0 (see figure 6*b*). The Padé approximant still exhibits a very good agreement with the probability densities for $\eta_0 = 5\times10^{-4}$ and 10^{-3}, which conform with (3.12), whereas there is a clear deviation for the higher-amplitude substrate families, $\eta_0 = 5\times10^{-3}$ and 10^{-2}.

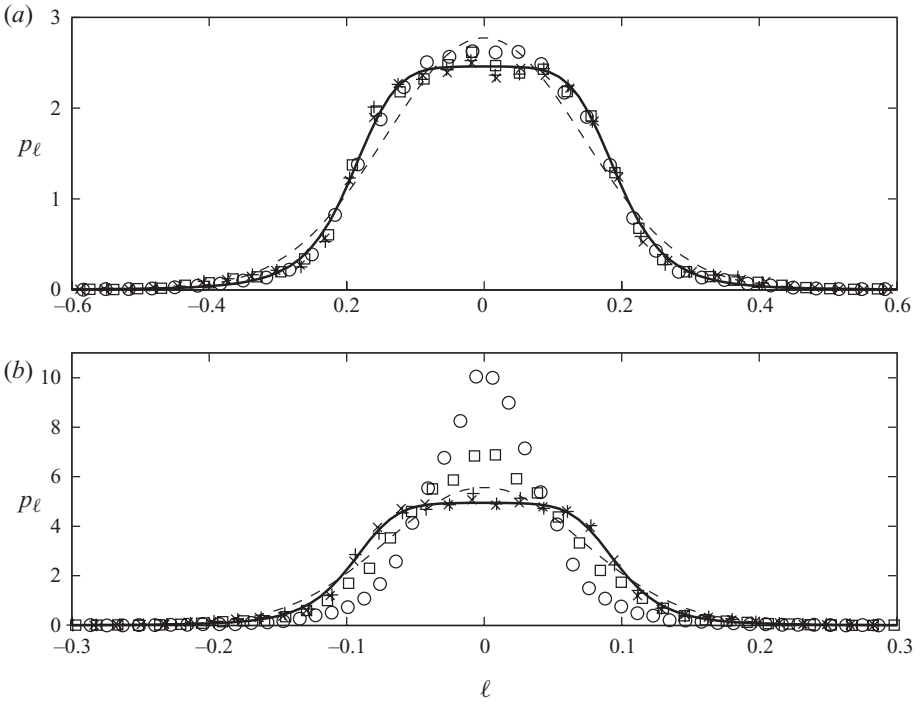

FIGURE 6. Probability density function of ℓ determined from numerical experiments using 2×10^4 substrate realizations for $\eta_0 = 5 \times 10^{-4}$ (+), 10^{-3} ($\times$), 5×10^{-3} (□) and 10^{-2} (○) with (*a*) $k_0 = 10$ and (*b*) $k_0 = 20$. The solid line shows the corresponding Padé approximant (4.15), whereas the dashed line is the corresponding normal density with the same variance.

5. Contact line fluctuation statistics

The extent to which wetting is affected by the substrate heterogeneities is determined by the statistics of the contact line fluctuation. The droplet shift measures the translation of the droplet away from some arbitrary origin, which has more physical content when the origin is fixed by the initial droplet shape in a dynamic setting. It is thus of interest to know whether statics alone can characterize the wetting properties of the substrate. Contrary to the droplet shift, we now have an explicit expression for the contact line fluctuations (3.11), which by the central limit theorem is expected to approach, at least to an approximation, a normal variable as $N \to \infty$ (Breiman 1992).

Hence, the statistical properties of ε are completely determined if its mean and variance are known. For determining the mean, we need to compute $\langle \alpha_m \sin k_m \ell + \beta_m \cos k_m \ell \rangle$. From (3.13), we see that ℓ depends on an infinite number of α_m and β_m values and it is thus expected that, on average, such dependence is weak. It is therefore reasonable to have $\langle \alpha_m \sin k_m \ell + \beta_m \cos k_m \ell \rangle \approx \langle \alpha_m \rangle \langle \sin k_m \ell \rangle + \langle \beta_m \rangle \langle \cos k_m \ell \rangle = 0$, as confirmed by numerical experiments. From this argument, an important statement follows, i.e. $\langle \varepsilon \rangle = 0$, from which one would infer that the wetting properties of the substrate are not altered on average by its spatial heterogeneities. This obviously would contradict experimental studies which suggest that substrate roughness does indeed alter wetting. This apparent inconsistency stems from the fact that the dynamics is not taken into account. Hence, the substrate wettability characteristics are the result of a dynamic spreading process and equilibrium considerations alone do not suffice to fully extract them. This is because in a dynamic setting the various droplet equilibria

may be either stable or unstable, as has been shown in the recent study of contact line dynamics on a spatially heterogeneous deterministic substrate by Savva & Kalliadasis (2009). Such distinction will be made in Part 2 (Savva, Pavliotis & Kalliadasis 2011), when a stability analysis is performed for the equilibria of ℓ. However, in the parameter regime we are presently considering, some statistical parameters are not affected by stability considerations and can be characterized through equilibrium considerations. For example, the second moment, which is identical to the variance, is given by

$$\mathrm{Var}[\varepsilon] = \frac{\eta_0^2}{4N}\sum_{m,n=1}^{N}[\langle\alpha_m\alpha_n \sin k_m\ell \sin k_n\ell\rangle + \langle\beta_m\beta_n \cos k_m\ell \cos k_n\ell\rangle + 2\langle\alpha_m\beta_n \sin k_m\ell \cos k_n\ell\rangle]F(k_m\sqrt{3})F(k_n\sqrt{3}). \quad (5.1)$$

On the basis of the independence of α_m and α_n, we take

$$\left\langle \alpha_m^2 \sin^2 k_m\ell + \beta_m^2 \cos^2 k_m\ell \right\rangle \approx 1, \quad (5.2)$$

and also assume that the cross-interaction terms $\langle\alpha_m\alpha_n \sin k_m\ell \sin k_n\ell\rangle$, $\langle\beta_m\beta_n \cos k_m\ell \cos k_n\ell\rangle$ and $\langle\alpha_m\beta_n \sin k_m\ell \cos k_n\ell\rangle$ are negligible compared to (5.2). Hence,

$$\begin{aligned}\mathrm{Var}\,[\varepsilon] &= \frac{\eta_0^2}{4}\int_0^1 [F(yk_0\sqrt{3})]^2\,\mathrm{d}y \\ &= \frac{\eta_0^2}{4}\left[\frac{k_0^4+3k_0^2-3}{2k_0^2} - \frac{7k_0^2-6}{4k_0^2}\cos(2\sqrt{3}k_0) - \frac{6k_0^2-37}{4}\,\mathrm{sinc}(2\sqrt{3}k_0)\right], \end{aligned} \quad (5.3)$$

whose asymptotic behaviour is

$$\mathrm{Var}[\varepsilon] \sim \frac{\eta_0^2k_0^2}{8}\left[1 - 3\,\mathrm{sinc}(2\sqrt{3}k_0) + O\left(k_0^{-2}\right)\right], \quad (5.4)$$

when $k_0 \gg 1$. A rigorous justification for the above steps has been given in § 7 of Part 2. We therefore find that the standard deviation of ε, $\sigma_\varepsilon = \sqrt{\mathrm{Var}[\varepsilon]}$, increases in a nearly linear fashion with respect to η_0k_0, which suggests that as the substrate becomes more rough, the contact line fluctuations tend to vary more widely from the mean fluctuation (in this case zero). The probability density of ε is therefore

$$p_\varepsilon(\epsilon) = \frac{1}{\sqrt{2\pi\sigma_\epsilon^2}}\exp\left(-\frac{\varepsilon^2}{2\sigma_\varepsilon^2}\right). \quad (5.5)$$

In figure 7 we plot the theoretically predicted probability density functions together with the corresponding probability densities obtained from numerical experiments using 2×10^4 realizations from substrate families with $\eta_0 = 5\times10^{-4}$ and $k_0 = 10$, 20, 40 and 80. We note the excellent agreement between theory and numerics, particularly for $k_0 = 10$, 20 and 40. However, when $k_0 = 80$, for which $\eta_0k_0^2 = 3.2$, the theory clearly overestimates the variance of ε. The dashed line shows the probability density of a normal variable having the same variance with that obtained from the numerical experiments with $k_0 = 80$, suggesting that the normality of ε persists, as the central limit theorem dictates.

The preceding analysis suggests that on average there is no substrate-induced hysteresis, when considering only the statics. It is nevertheless instructive to see what can be said about the apparent contact angle. Since the amplitude of the topography

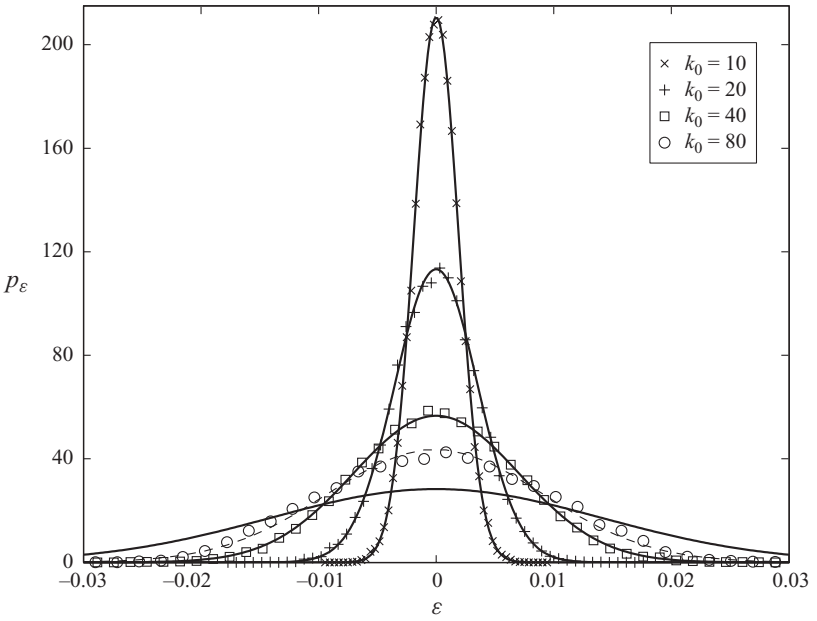

FIGURE 7. Comparison of the numerically determined probability density function of ε (symbols) with the theoretically predicted normal density (solid lines) for substrate families with $\eta_0 = 5 \times 10^{-4}$ and $k_0 = 10$, 20, 40 and 80. All densities have zero mean, implying a zero net effect on wetting. Apart from $k_0 = 80$, the agreement between theory and numerical experiments is excellent. The family for which $k_0 = 80$ clearly violates (3.12), but the contact line fluctuation is still a normally distributed random variable as the normal density with the same variance, depicted by the dashed line, suggests.

is small, we may write (3.5*a*) as

$$\theta_{app} = 1 - \frac{\eta_a' - \eta_b'}{2} + O(\eta_0), \tag{5.6}$$

where we identified $\theta_{app} = 3/d^2$ as the apparent contact angle. This implies that

$$\sigma_\theta^2 = \mathrm{Var}\left[\theta_{app}\right] = \mathrm{Var}\left[\frac{\eta_a' - \eta_b'}{2}\right] = \frac{\eta_0^2 k_0^2}{6} + O\left(k_0\right) = r - 1, \tag{5.7}$$

where r is the substrate roughness coefficient given in (2.5). This behaviour is confirmed in figure 8, where we plot σ_θ as a function of $\eta_0 k_0$ for substrate families with different characteristic amplitudes and wavenumbers. We note that provided (3.12) is satisfied and $\eta_0 k_0 \lessapprox 10^{-2}$, σ_θ grows almost linearly. As the substrate becomes more rough, however, the increase is significantly slower. Such a plot also suggests that variations in the substrate topography introduce an uncertainty in the observed apparent contact angle that tends to increase with substrate roughness.

6. Generalization to arbitrary stationary random functions

The preceding analysis was specific to band-limited white-noise substrate representations. Here, we examine a generalization to arbitrary substrate families

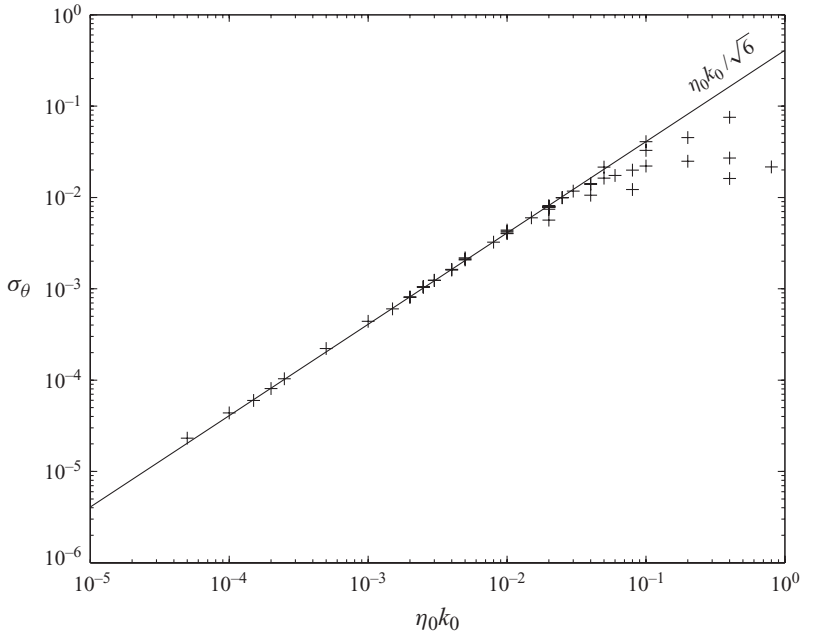

FIGURE 8. Standard deviation of the apparent contact angle, σ_θ, as a function of $\eta_0 k_0$ for various substrate families. Provided that (3.12) is satisfied and $\eta_0 k_0 \lessapprox 10^{-2}$, σ_θ follows the theoretically predicted result, $\sigma_\theta \approx \eta_0 k_0/6$.

of the form

$$\eta(x) = \sum_{m=1}^{+\infty} (\alpha_m \sin \kappa_m x + \beta_m \cos \kappa_m x) \sqrt{S(\kappa_m)\,\Delta\kappa}, \tag{6.1}$$

where now the κ_m values are discrete wavenumbers that satisfy $\kappa_m - \kappa_{m-1} = \Delta\kappa$ with $\kappa_1 = 0$. The function $S(\kappa)$ corresponds to the spectral density function of the random profile $\eta(x)$, which, when appropriately normalized with $\int_0^{+\infty} S(\kappa)\,\mathrm{d}\kappa$, can be viewed as a probability density for the random frequency content of $\eta(x)$ (VanMarcke 1983). For example, the band-limited white-noise substrates have a spectral density of the form

$$S_0(\kappa) = \begin{cases} \eta_0^2/k_0, & \kappa \in [0, k_0], \\ 0, & \kappa \notin [0, k_0], \end{cases} \tag{6.2}$$

and consequently $S_0(\kappa)/\eta_0^2$ may be regarded as a uniform probability density function, which confirms our earlier assertion that with this representation all wavenumbers within $[0, k_0]$ are equally probable to be present in a random profile realization.

Substituting (6.1) and (3.6) in (3.5), followed by a linearization using (3.10), yields the system of equations

$$\varepsilon = \frac{1}{2} \sum_{m=1}^{+\infty} (\alpha_m \sin \kappa_m \ell + \beta_m \cos \kappa_m \ell) F(\kappa_m \sqrt{3}) \sqrt{S(\kappa_m)\Delta\kappa}, \tag{6.3a}$$

$$0 = \sum_{m=1}^{N} (\alpha_m \cos \kappa_m \ell - \beta_m \sin \kappa_m \ell) G(\kappa_m \sqrt{3}) \sqrt{S(\kappa_m)\Delta\kappa}, \tag{6.3b}$$

which is identical to (3.11) and (3.13) when $S(\kappa)$ is given by (6.2). For these more general representations and for the sake of illustration of our procedure, we only investigate the variance of ε. We thus seek the leading-order expression in the limit of large characteristic wavenumbers, which allows us to take $F(\kappa) \sim -\kappa \sin\kappa$. Proceeding as before, the variance of ε is given from

$$\sigma_\varepsilon^2 \sim \frac{3}{4}\int_0^{+\infty} \kappa^2 S(\kappa)\sin^2(\kappa\sqrt{3})\,\mathrm{d}\kappa. \tag{6.4}$$

The above equation may be expressed in terms of the autocovariance function of the first derivative of $\eta(x)$, namely

$$\sigma_\varepsilon^2 \sim \tfrac{3}{8}[R(0) - R(2\sqrt{3})], \tag{6.5}$$

where

$$R(\tau) = \langle \eta'(x)\,\eta'(x+\tau)\rangle = \int_0^{+\infty} \kappa^2 S(\kappa)\cos\kappa\tau\,\mathrm{d}\kappa. \tag{6.6}$$

Hence, it is apparent that the profile representation is completely determined if we know the height distribution and the spectral density of the substrate (Whitehouse & Archard 1970). From our discussion in § 2, it is reasonable to assume that the substrate heights are normally distributed, and by choosing the appropriate functional form for the spectral density it suffices to compute the statistics of ε.

Predicting theoretically the spectral density is usually a formidable task especially because the several processes involved in surface formation introduce surface features in a rather unpredictable manner (Thomas 1999). Hence, approximations to spectral densities are typically obtained from measured profiles. Substrate profilometry techniques such as stylus-based or optical instruments are limited in terms of resolution and accuracy. For example, stylus measurements are sensitive to the stylus size (e.g. Poon & Bhushan 1995), typically in the submicron regime. Hence, with a large stylus tip, rapidly varying substrate features may appear to be cusped. In addition, stylus instruments, such as atomic force microscopy, may scratch the substrate or give erroneous readings when the rate at which the substrate is swept is high and the stylus fails to maintain contact with the substrate, whereas the accuracy of measurements by optical techniques depends on whether the substrate has homogeneous optical properties (Bhushan 2000).

Hence, to make theoretical progress in rough-substrate characterization problems, the experimentally obtained spectral densities are usually fitted with relatively simple functional forms. Whitehouse & Archard (1970) were the first to propose the use of a spectral density of the form

$$S(\kappa) = \frac{A}{1+\kappa^2/\kappa_c^2}, \tag{6.7}$$

where A and κ_c are constants and $\eta(x)$ has an exponential autocovariance function, $\langle\eta(x)\eta(x+\tau)\rangle = \pi\kappa_c A\mathrm{e}^{-\kappa_c|\tau|}/2$. More recently, Katzav, Adda-Bedia & Derrida (2007) derived theoretically a spectral density of the above form for surfaces resulting from a propagating crack. Sayles & Thomas (1978) argued against the stationarity assumption of a rough substrate based on measurements of the variance of $\eta(x)$, which appeared to be non-unique and dependent on the size of the sample substrate considered. By using measurements taken over a broad range of length scales, they proposed a universal power-law dependence for the spectral density of the form that

scales like $\sim \kappa^{-2}$. Similar power-law scalings were derived by Edwards & Wilkinson (1982) for the long-limit asymptotics for surfaces generated by a deposition process.

This work motivated a series of further studies that attempted to offer a fractal description for a rough substrate (see e.g. Majumdar & Tien 1990). Self-affine fractals, i.e. structures that exhibit self-similarity at different length scales when anisotropically stretched (see figure 9), were found to be particularly appealing by advocates of the fractal representation, because they naturally arise with a power-law spectral density. In practice, however, it is impossible for a real substrate to have a persistent fractal structure for all wavenumbers, because a natural or artificial process cannot operate over an infinite range of wavenumbers (Thomas 1999). Evidence against the universality of a power-law spectral density was offered in the experiments by Mulvaney *et al.* (1989), who found that spectral densities were better represented with functions of the form (6.7), attributing deviations from this form to inadvertent changes in the substrate fabrication mechanisms. Whitehouse (2001) argued that a power-law spectral density was wrongly extracted from a relatively narrow bandwidth of wavenumbers, imposed by the previously mentioned limitations in substrate roughness measurements. To overcome these limitations, a 'multifractal' representation was introduced whose spectral density may exhibit different power laws at different scales (e.g. Bhushan & Majumdar 1992). But to date a general consensus for a rough substrate representation is lacking, primarily because of the wide variations in the characteristics of the several processes involved in substrate formation.

In what follows, we shall demonstrate that the actual spectral density chosen for the substrate does not qualitatively affect the statistics of droplet equilibria with respect to the characteristic amplitude, η_0, and wavenumber, k_0. To do this, we examine the variances of the contact line fluctuation for two popular choices, namely a 'bell-shaped' spectral density of the form (6.7) and a family of power-law spectral densities that give rise to a fractal structure. However, cutoffs must be imposed so that the resulting random substrate families remain continuous and differentiable. In practice, cutoffs naturally arise since the spectrum of measured substrate profiles lies within a finite bandwidth of wavenumbers, limited between a small wavenumber, because of the sample size substrate considered, and a large wavenumber, imposed by the resolution of the instrument, e.g. the stylus size.

6.1. *'Bell' spectral density*

We first consider a spectral density that depends on three parameters, η_0, k_0 and s, of the form (Whitehouse & Archard 1970; Mulvaney *et al.* 1989)

$$S_1(\kappa) = \begin{cases} A_1 \dfrac{1}{1 + \left(\dfrac{\kappa}{sk_0}\right)^2}, & \kappa \in [0, k_0], \\ 0, & \kappa \notin [0, k_0], \end{cases} \tag{6.8}$$

where setting $A_1 = \eta_0^2/(sk_0 \arctan s^{-1})$ ensures that $\int_0^{+\infty} S_1(\kappa)\,\mathrm{d}\kappa = \eta_0^2$. The extra parameter s satisfies $S(sk_0) = A_1/2$, i.e. it determines the breadth of $S_1(\kappa)$ (see figure 10*a*). Again, a cutoff wavenumber was introduced so that the higher derivatives remain continuous. Integrating (6.3*a*) by parts gives the variance of ε, σ_1^2, to $O(\eta_0^2 k_0^0)$,

$$\frac{\sigma_1^2}{\bar{\sigma}_\varepsilon^2} \sim \lambda_1^2 \left[1 - \frac{\operatorname{sinc} 2k_0\sqrt{3}}{(s^2+1)(1 - s \arctan s^{-1})}\right], \tag{6.9}$$

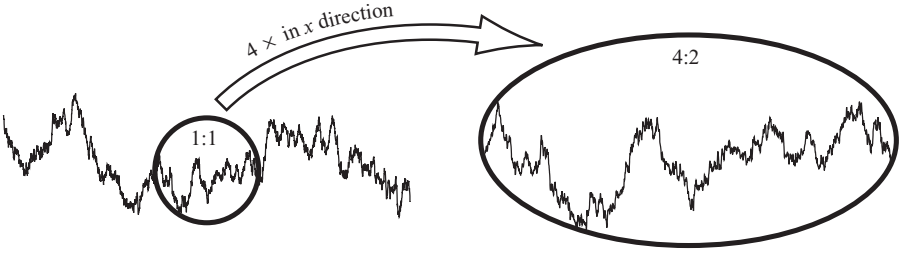

FIGURE 9. Illustration of statistical self-affinity when the fractal dimension is $D = 1.5$. Observing the substrate at a different length scale by an appropriate anisotropic magnification yields a profile with identical statistical properties as the original one.

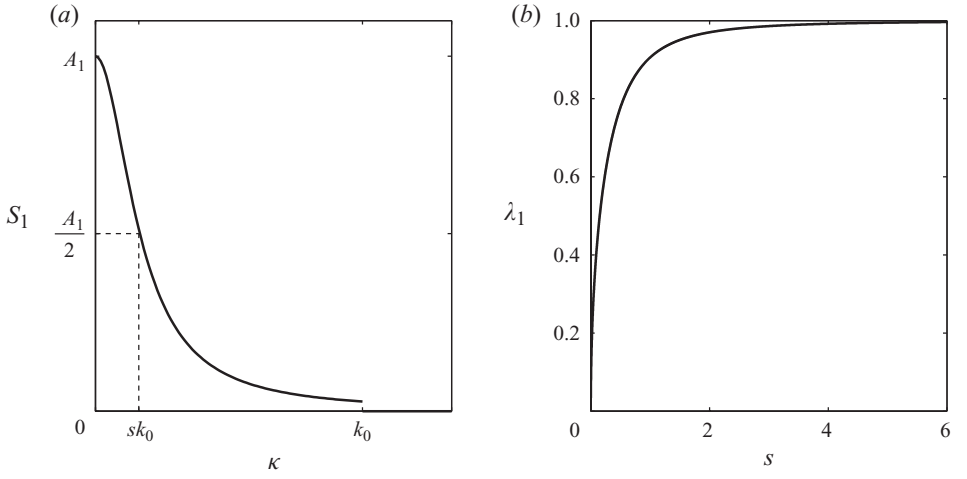

FIGURE 10. (*a*) Form of 'bell-shaped' spectral density (6.8); (*b*) plot of the ratio of the leading-order standard deviation of ε to the leading-order standard deviation for the band-limited white noise.

where $\bar{\sigma}_\varepsilon^2 = \eta_0^2 k_0^2/8$ is the leading-order variance for the band-limited white noise and $\lambda_1^2 = 3s^2[(s \arctan s^{-1})^{-1} - 1]$. Given that we are mainly interested in $k_0 \gg 1$, we will neglect sinc $2k_0\sqrt{3}$ compared with 1. Figure 10(*b*) depicts λ_1 as a function of the extra parameter s. An asymptotic behaviour towards 1, the band-limited white-noise case, is evident in the figure. As $s \to 0$, the substrate becomes flat and as a consequence there are no contact line fluctuations, thus justifying why $\sigma_1^2 \to 0$.

6.2. *Fractal substrates*

Majumdar & Tien (1990) utilized the Weierstrass–Mandelbrot function to characterize a fractal substrate that exhibits self-affinity in the form given by

$$f(x) = \bar{f} \sum_{n=-\infty}^{+\infty} \frac{\cos 2\pi\gamma^n x}{\gamma^{(2-D)n}}, \tag{6.10}$$

where $\gamma > 1$ and $\bar{f}$ are arbitrary parameters and $1 < D < 2$ corresponds to the fractal dimension, even though there is no rigorous proof for this (Mandelbrot 1982). This function, which resembles a Fourier series whose wavenumbers increase in a geometric rather than in a linear progression, is everywhere continuous with discontinuous derivatives (Berry & Lewis 1980). Furthermore, $f(x)$ can be easily shown to be

self-affine, satisfying

$$f(x) = \gamma^{2-D} f(x/\gamma). \tag{6.11}$$

This would mean that if we magnify a portion of the curve of $f(x)$ by a factor γ in the x-direction, we will get a curve that is self-similar to the original one if we stretch it in the y-direction by γ^{2-D}. It is noteworthy that the roughness exponent, ζ, introduced in § 2 to usually describe fractal-like substrates is related to the fractal dimension by the relation $\zeta = 2 - D$.

In the work of Majumdar & Tien (1990), a rough substrate was assumed to have the above deterministic form and statistical parameters were deduced from it. However, since we are interested in random substrate realizations, we consider a substrate of the form

$$\eta(x) = \bar{A}_2 \sum_{m=-\infty}^{+\infty} \left(\alpha_m \frac{\sin 2\pi\gamma^m x}{\gamma^{(2-D)m}} + \beta_m \frac{\cos 2\pi\gamma^m x}{\gamma^{(2-D)m}} \right) \sqrt{\Delta m}, \tag{6.12}$$

where $\bar{A}_2$ is a constant and $\Delta m = 1$. Here we no longer have exact affine similarity due to the randomness in the generation of the profile and hence self-affinity is now meant to exist in a statistical sense, i.e. the probability distributions of $\eta(x)$ are identical if appropriately re-scaled. This is illustrated in figure 9 for a realization of $\eta(x)$ when $\gamma = 4$ and $D = 3/2$. If we magnify a portion of the curve four times in the x-direction, statistical self-affinity between the magnified portion and the original fractal can only be achieved if we also magnify that portion by $4^{2-3/2} = 2$ times in the y-direction. The representation in (6.12) has a discrete spectrum and we would like to appropriately re-cast (6.12) in the form of (6.1), which has a continuous spectrum as $\Delta k \to 0$. To do this, let

$$\gamma^m = \frac{k_m}{2\pi} \Rightarrow \Delta m = \frac{\Delta k}{2\pi\gamma^m \ln\gamma}, \tag{6.13}$$

so that

$$\eta(x) = \sum_{m=1}^{+\infty} (\alpha_m \sin k_m x + \beta_m \cos k_m x) \sqrt{\frac{A_2 \Delta k}{k_m^{5-2D}}}, \tag{6.14}$$

where $A_2 = \bar{A}_2^2/((2\pi)^{2D-4} \ln\gamma)$, which is in the form of (6.1) with spectral density $S_2(\kappa) \propto \kappa^{2D-5}$. Considering a limited bandwidth of wavelengths to ensure differentiability, we define the spectral density

$$S_2(\kappa) = \begin{cases} A_2 \kappa^{2D-5}, & \kappa \in [g k_0, k_0], \\ 0, & \kappa \notin [g k_0, k_0], \end{cases} \tag{6.15}$$

where $0 \leqslant g \leqslant 1$ (see figure 11*a*). Letting

$$A_2 = \begin{cases} -\dfrac{\eta_0^2}{\ln g}, & D = 2, \\ \dfrac{(4-2D)(k_0 g)^{4-2D} \eta_0^2}{1 - g^{4-2D}}, & D \neq 2, \end{cases} \tag{6.16}$$

so that $\int_{g k_0}^{k_0} S_2(\kappa)\, \mathrm{d}\kappa = \eta_0^2$, gives a representation that depends on four parameters, namely k_0, g, D and η_0. Integration by parts in (6.3*a*) yields the variance of the

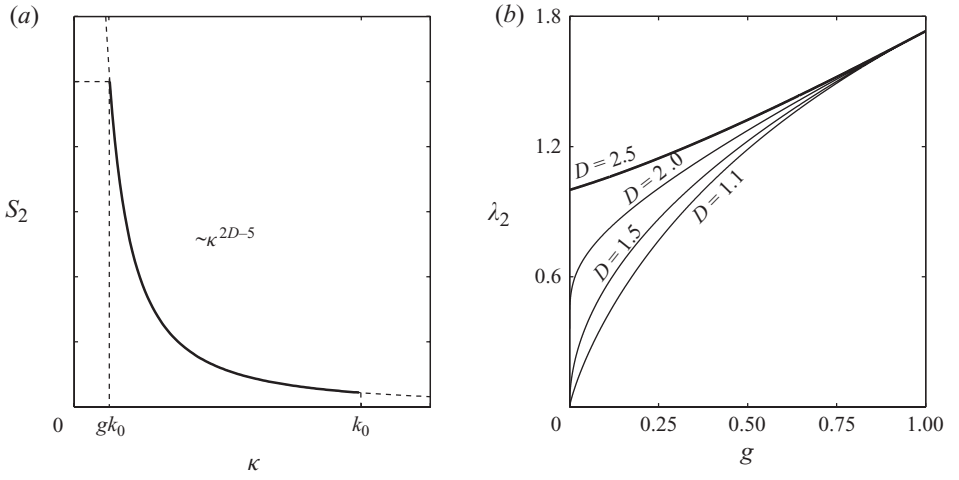

FIGURE 11. (*a*) Form of the power-law spectral density (6.15); (*b*) plot of the ratio of the leading-order standard deviation of ε to the leading-order standard deviation for the band-limited white noise.

contact line fluctuations, σ_2^2, to $O(\eta_0^2 k_0^0)$,

$$\frac{\sigma_2^2}{\bar{\sigma}_\varepsilon^2} \sim \lambda_2^2 \left\{ 1 - \frac{2(D-1)}{1-g^{2(D-1)}} \left[\operatorname{sinc}(2k_0\sqrt{3}) - g^{2(D-1)} \operatorname{sinc}(2gk_0\sqrt{3}) \right] \right\}, \tag{6.17}$$

where

$$\lambda_2^2 = \begin{cases} \dfrac{3(g^2-1)}{2\ln g}, & D = 2, \\ \dfrac{3g^2(2-D)\left(g^{2(1-D)}-1\right)}{(D-1)\left(1-g^{2(2-D)}\right)}, & D \neq 2. \end{cases} \tag{6.18}$$

This prefactor depends only on the newly introduced parameters and the overall behaviour of the variance does not change with respect to η_0 and k_0. Figure 11(*b*) shows λ_2 as a function of g for $1 < D \leqslant 5/2$. We readily see that as $g \to 0$, $\sigma_2^2 \to 0$ unless $D = 5/2$, implying that the substrate realizations become flat in this limit. The case $D = 5/2$, $g = 0$ is precisely the band-limited white-noise case represented by (2.1). As $g \to 1$, all curves have a common limit because a single harmonic, k_0, is sampled.

7. Conclusions

We have analysed the statistics of droplet equilibria on random topographical substrates. The first step was the development of an appropriate representation of such substrates as a stationary random function that is equivalent to white noise undergoing through a low-pass filter. Families of infinitely differentiable random substrates are conveniently described by a characteristic amplitude and wavenumber. Our substrate representation can be satisfactorily used to model a real substrate with random asperities.

The long-wave approximation yields an equation governing droplet equilibria and subject to wall conditions and constant area constraint. It can be readily solved to yield two equations for the locations of the contact lines. These are linearized about the flat-substrate equilibrium to obtain a set of equations for the droplet radius and

shift along the substrate. The droplet radius is found to be well-approximated by a normal variable whose standard deviation appears to grow with substrate roughness to leading order in the substrate characteristics.

Determining the droplet shift statistics is more difficult due to its resemblance to a first-passage problem. However, for weakly asymmetric substrates, the shift approaches a Cauchy random variable, whereas for fully asymmetric ones the probability density is not given by a known, analytical form, but is nevertheless estimated by a Padé approximant. Generalization to arbitrary stationary random functions reveals no qualitative differences with respect to the characteristic amplitude and wavenumber.

Our theoretical predictions are confirmed by numerical experiments which also suggest that on average the wetting properties are not affected by the substrate roughness. This result is due to the fact that our analysis is restricted to the droplet equilibria only. Indeed, considering static configurations only cannot distinguish between stable and unstable ones and adequately characterize the attainable droplet equilibria. In reality, only the stable equilibria are observable, and to account for this we must consider the dynamics. This is the subject of Part 2.

We acknowledge financial support from EPSRC Platform Grant No. EP/E046029 and ERC Advanced Grant No. 247031.

Appendix. Continuity of substrate representation and its derivatives

To prove the continuity of the random substrate and all its derivatives, we invoke Kolmogorov's continuity theorem. If a stochastic process satisfies its requirements, the theorem guarantees the existence of a continuous version for the stochastic process (Øksendal 2003).

Obviously, continuity of $\eta(x)$ and its derivatives is guaranteed for all finite N. What we are interested in is the limit as $N\to\infty$. We carefully prove this for $\eta^{(n)}(x)$. To proceed, we consider

$$\langle|\eta^{(n)}(x+h)-\eta^{(n)}(x)|^2\rangle = \lim_{N\to\infty}\frac{4\eta_0^2}{N}\left\langle\left|\sum_{m=1}^{N}\left(\frac{mk_0}{N}\right)^n\sin\left(\frac{mk_0h}{2N}\right)\right.\right.$$
$$\left.\left.\times\left\{\bar\alpha_m\cos\frac{mk_0\,(2x+h)}{2N}+\bar\beta_m\sin\frac{mk_0\,(2x+h)}{2N}\right\}\right|^2\right\rangle, \quad (A\,1)$$

where depending on n, $\bar\alpha_m$ and $\bar\beta_m$ can be either $\pm\alpha_m$ or $\pm\beta_m$. For example, when $n=0$, we have $\bar\alpha_m=\alpha_m$ and $\bar\beta_m=-\beta_m$, for $n=1$ we have $\bar\alpha_m=-\beta_m$ and $\bar\beta_m=-\alpha_m$, for $n=2$ we have $\bar\alpha_m=-\alpha_m$ and $\bar\beta_m=\beta_m$ and so on. Taking the mean of the expression above together with the mutual independence of all random variables α_m and β_m allows us to write

$$\langle|\eta^{(n)}(x+h)-\eta^{(n)}(x)|^2\rangle = \lim_{N\to\infty}\frac{4\eta_0^2}{N}\sum_{m=1}^{N}\left(\frac{mk_0}{N}\right)^{2n}\sin^2\left(\frac{mk_0h}{2N}\right)$$
$$\leqslant \lim_{N\to\infty}\frac{\eta_0^2k_0^{2n+2}h^2}{N}\sum_{m=1}^{N}\left(\frac{m}{N}\right)^{2n+2}$$
$$\leqslant \frac{\eta_0^2k_0^{2n+2}h^2}{2n+3}\quad\forall h, \quad (A\,2)$$

upon converting the sum into an integral. We readily see that the requirements of Kolmogorov's continuity theorem are satisfied with $D = \eta_0^2 k_0^{2n+2} h^2/(2n+3)$, $c_1 = 2$ and $c_2 = 1$. Hence, the chosen form for the substrate is a continuous and infinitely differentiable function, provided that k_0 is finite. The limit $k_0 \to \infty$ renders the above calculation invalid, since $\eta(x)$ approaches white noise, a nowhere differentiable random function.

REFERENCES

Baker, G. A. & Graves-Morris, P. R. 1996 *Padé Approximants*. Cambridge University Press.

Barabási, A.-L. & Stanley, H. E. 1995 *Fractal Concepts in Surface Growth*. Cambridge University Press.

Berry, M. V. & Lewis, Z. V. 1980 On the Weierstrass–Mandelbrot fractal function. *Proc. R. Soc. Lond.* A **370** (1743), 459–484.

Bhushan, B. 2000 Surface roughness analysis and measurement techniques. In *Modern Tribology Handbook* (ed. B. Bhushan), vol. 1, chap. 2, pp. 49–119. CRC Press LLC.

Bhushan, B. & Majumdar, A. 1992 Elastic–plastic model for bifractal surfaces. *Wear* **153**, 53–64.

Bico, J., Tordeux, C. & Quéré, D. 2001 Rough wetting. *Europhys. Lett.* **55** (2), 214–220.

Blake, T. D. 1993 Dynamic contact angles and wetting kinetics. In *Wettability* (ed. J. C. Berg), pp. 251–310. Marcel Dekker.

Blossey, R. 2003 Self-cleaning surfaces–virtual realities. *Nature Mater.* **2**, 301–306.

Bonn, D., Eggers, J., Indekeu, J., Meunier, J. & Rolley, E. 2009 Wetting and spreading. *Rev. Mod. Phys.* **81**, 739–805.

Borgs, C., De Coninck, J., Kotecký, R. & Zinque, M. 1995 Does the roughness of the substrate enhance wetting? *Phys. Rev. Lett.* **74** (12), 2292–2294.

Breiman, L. 1992 *Probability*. SIAM.

Callies, M. & Quéré, D. 2005 On water repellency. *Soft Matt.* **1**, 55–61.

Chung, J. Y., Youngblood, J. P. & Stafford, C. M. 2007 Anisotropic wetting on tunable micro-wrinkled surfaces. *Soft Matt.* **3**, 1163–1169.

Cox, R. G. 1983 The spreading of a liquid on a rough solid surface. *J. Fluid Mech.* **131**, 1–26.

Dussan V., E. B. 1979 On the spreading of liquids on solid surfaces: static and dynamic contact lines. *Annu. Rev. Fluid Mech.* **11**, 371–400.

Edwards, S. F. & Wilkinson, D. R. 1982 The surface statistics of a granular aggregate. *Proc. R. Soc. Lond.* A **381**, 17–31.

Geary, R. C. 1930 The frequency distribution of the quotient of two normal variates. *R. Stat. Soc. J.* **93**, 442–446.

de Gennes, P.-G. 1985 Wetting: statics and dynamics. *Rev. Mod. Phys.* **57** (3), 827–863.

de Gennes, P.-G., Brochard-Wyart, F. & Quéré, D. 2003 *Capillarity and Wetting Phenomena*. Springer.

Good, R. J. 1952 A thermodynamic derivation of Wenzel's modification of Young's equation for contact angles; together with a theory of hysteresis. *J. Am. Chem. Soc.* **74**, 5041–5042.

Greenwood, J. A. & Williamson, J. B. P. 1966 Nominally flat surfaces. *Proc. R. Soc. Lond.* A **295** (1442), 310–319.

Hazlett, R. D. 1990 Fractal applications: wettability and contact angle. *J. Colloid Interface Sci.* **173** (2), 527–533.

Hazlett, R. D. 1992 On surface roughness effects in wetting phenomena. *J. Adhes. Sci. Technol.* **6** (6), 625–633.

Hitchcock, S. J., Carroll, N. T. & Nicholas, M. G. 1981 Some effects of substrate roughness on wettability. *J. Mater. Sci.* **16**, 714–732.

Huh, C. & Mason, S. G. 1977 Effects of surface roughness on wetting (theoretical). *J. Colloid Interface Sci.* **60** (1), 11–38.

Jansons, K. M. 1985 Moving contact lines on a two-dimensional rough surface. *J. Fluid Mech.* **154**, 1–28.

Joanny, J. & de Gennes, P.-G. 1984 A model for contact angle hysteresis. *J. Chem. Phys.* **81** (1), 552–562.

Johnson, R. E. & Dettre, R. H. 1964 Contact angle hysteresis. I. Study of an idealized rough surface. In *Advances in Chemistry Series,* vol. 43, *Contact Angle, Wettability and Adhesion* (ed. F. M. Fowkes), pp. 112–135. American Chemical Society.

van Kampen, N. G. 2007 *Stochastic Processes in Physics and Chemistry*, 3rd edn. Elsevier.

Katzav, E., Adda-Bedia, M. & Derrida, B. 2007 Fracture surfaces of heterogeneous materials: a 2D solvable model. *Europhys. Lett.* **78**, 46006.

Krishnamoorthy, K. 2006 *Handbook of Statistical Distributions with Applications*. Chapman & Hall/CRC.

Longuet-Higgins, M. S. 1958 On the intervals between successive zeros of a random function. *Proc. R. Soc. Lond.* A **246**, 99–118.

Majumdar, A. & Tien, C. L. 1990 Fractal characterization and simulation of rough surfaces. *Wear* **136**, 313–327.

Mandelbrot, B. B. 1982 *The Fractal Geometry of Nature*. Freeman.

McHale, G. 2007 Cassie and Wenzel: were they really so wrong? *Langmuir* **23**, 8200–8205.

Mulvaney, D. J., Newland, D. E. & Gill, K. F. 1989 A complete description of surface texture profiles. *Wear* **132**, 173–182.

Øksendal, B. 2003 *Stochastic Differential Equations*, 6th edn. Springer.

Oliver, J. F., Huh, C. & Mason, S. G. 1977 The apparent contact angle of liquids on finely-grooved solid surfaces – a SEM study. *J. Adhes.* **8**, 223–234.

Oliver, J. F., Huh, C. & Mason, S. G. 1980 An experimental study of some effects of solid surface roughness on wetting. *Colloids Surf.* **1**, 79–104.

Palasantzas, G. & De Hosson, J. Th. M. 2001 Wetting on rough surfaces. *Acta Mater.* **49**, 3533–3538.

Pomeau, Y. & Vannimenus, J. 1985 Contact angle on heterogeneous surfaces: weak heterogeneities. *J. Colloid Interface Sci.* **104** (2), 477–488.

Poon, C. Y. & Bhushan, B. 1995 Comparison of surface roughness measurements by stylus profiler, AFM and non-contact optical profiler. *Wear* **190**, 76–88.

Rice, S. O. 1945 The mathematical analysis of random noise. *Bell Syst. Tech. J.* **24**, 46–156.

Robbins, M. O. & Joanny, J. F. 1987 Contact angle hysteresis on random surfaces. *Europhys. Lett.* **3** (6), 729–735.

Roberts, A. P. & Torquato, S. 1999 Chord-distribution functions of three-dimensional random media: approximate first-passage times of Gaussian processes. *Phys. Rev.* E **59** (5), 4953–4963.

Savva, N. & Kalliadasis, S. 2009 Two-dimensional droplet spreading over topographical substrates. *Phys. Fluids* **21**, 092102.

Savva, N., Pavliotis, G. A. & Kalliadasis, S. 2011 Contact lines over random topographical substrates. Part 2. Dynamics. *J. Fluid Mech.* **672**, 384–410.

Sayles, R. & Thomas, T. R. 1978 Surface topography as a non-stationary random process. *Nature* **271**, 431–434.

Shibuichi, S., Onda, T., Satoh, N. & Tsujii, K. 1996 Super water-repellent surfaces resulting from fractal structure. *J. Phys. Chem.* **100**, 19512–19517.

Thomas, T. R. 1999 *Rough Surfaces*, 2nd edn. Imperial College Press.

VanMarcke, E. 1983 *Random Fields: Analysis and Synthesis*. MIT Press.

Wenzel, R. N. 1936 Resistance of solid surfaces to wetting by water. *Ind. Engng Chem.* **28**, 988–994.

Whitehouse, D. J. 2001 Fractal or fiction. *Wear* **249**, 345–353.

Whitehouse, D. J. & Archard, J. F. 1970 The properties of random surfaces of significance in their contact. *Proc. R. Soc. Lond.* A **316** (1524), 97–121.

Zeitak, R. 1997 Short time expansion for first-passage distributions. *Phys. Rev.* E **56** (3), 2560–2567.

Zhou, X. B. & De Hosson, J. Th. M. 1995 Influence of surface roughness on the wetting angle. *J. Mater. Res.* **10** (8), 1984–1992.